Research Article

Improvement of elevated-temperature strength and recrystallization resistance via Mn-containing dispersoid strengthening in Al-Mg-Si 6082 alloys

Chen Li[1], Kun Liu [1]*, and X.-Grant Chen[1]

[1]*Department of Applied Science, University of Québec at Chicoutimi, Chicoutimi, QC G7H 2B1, Canada*

[Received ; received in revised form ; Accepted]

* Corresponding author. Prof., Ph.D.; Tel.: +01 4185455011 ext. 7112.

E-mail address: kun.liu@uqac.ca (Kun Liu).

The precipitation behavior of Mn-containing dispersoids in Al-Mg-Si 6082 alloys with different Mn contents (0, 0.5 and 1.0 wt.%) during various heat treatments (300-500 ℃) was investigated. The effects of dispersoids on elevated-temperature strength and recrystallization resistance during hot-rolling and post-rolling annealing were evaluated. The results showed that the dispersoids in the Mn-containing alloys (0.5 and 1.0%) began to precipitate at 350 ℃ and reached the optimum conditions after 2-4 h at 400 ℃. However, the dispersoids coarsened with increasing holding time at temperatures above 450 ℃. After the peak precipitation treatment at 400 ℃ for 2 h, the yield strength at 300 ℃ increased from 28 MPa (base alloy free of Mn) to 55 MPa (alloy with 0.5% Mn) and 70 MPa (alloy with 1% Mn), respectively, demonstrating a significant dispersoid strengthening effect at elevated temperature. In addition, the dispersoids were thermally stable at 300 ℃ for up to 1000 h holding owing to its relative high precipitation temperature (350-400 ℃), leading to the superior constant mechanical performance at elevated temperature during the long service life. During hot rolling and post-rolling annealing, the presence of a large amount of dispersoids results in the higher Zener drag P_Z compared with base alloy and then significantly improved the recrystallization

resistance. The alloy containing 0.5% Mn exhibited the highest recrystallization resistance among three experimental alloys studied during the post-rolling process, likely resulted from the lower coarsening rate of dispersoids and the lower dispersoids free zone.

Key words: Al-Mg-Si 6082 alloy; Mn addition; Dispersoid precipitation; Elevated-temperature strength; Recrystallization resistance

1. Introduction

Al-Mg-Si 6xxx aluminum alloys are one of the most popular aluminum wrought alloys with a wide range of applications in the aircraft, automotive and construction industries due to their high strength to weight ratio, excellent corrosion resistance and low cost [1-3]. Recently, there have been increasing demands for aluminum alloys to be applied at elevated temperatures (250-350 ℃) in the automotive industries. However, the mechanical properties of 6xxx alloys deteriorate rapidly due to the coarsening and dissolution of traditional hardening precipitates of Mg_2Si at 250-350 ℃ [4]. In general, the 6xxx alloys are subjected to the rolling and extrusion processes to achieve a desirable shape. The occurrence of recrystallization during hot deformation inevitably weakens the mechanical strength of the final products. Therefore, studies concerning the improvement of the elevated-temperature properties and recrystallization resistance of 6xxx alloys are of great technical interest.

Introducing the thermally stable dispersoids via appropriate alloying elements and heat treatments is reported to be one of the most efficient and applicable approaches to enhance the elevated-temperature properties of aluminum alloys. It has been reported that the yield strength (YS) at 300 ℃ of Al-Mn-Mg 3004 alloys could be improved by 42% in comparison to that of the as-homogenized sample due to the formation of dispersoids and their excellent thermal stability [5]. On the other hand, the dispersoids are well recognized on retarding recovery and inhibiting recrystallization during hot deformation and post-deformation heat treatment [3, 6-9]. In the AA6013 alloy [10], it was found that the recrystallization resistance during hot rolling and post-deformation heat treatment increased due to the increasing Zener-drag force induced by Mn-containing

dispersoids. Generally, the efficiency of these dispersoids is highly dependent on their size and distributions. The dispersoids with fine size and dense distribution are considered to contribute to superior strength at elevated temperature and a high inhibition effect on recrystallization [11]. The formation of thermally stable dispersoids can be promoted by alloying elements, such as Mn, Fe and Mo [12-14], and proper heat treatment parameters [3]. However, limited research has been performed in 6xxx alloys about the evolution of dispersoids at different heat treatments and their influence on the elevated-temperature properties. In addition, although several works have addressed the effect of secondary particles on recrystallization during annealing [15-18], the impact of thermally stable dispersoids on the recrystallization resistance during a thermomechanical process and post-deformation heat treatment in 6xxx alloys is less clear.

In the present work, Al-Mg-Si 6082 alloys with different Mn contents (0 to 1 wt. %) were subjected to various heat treatments from 300 to 500 ℃ for different soaking times. The investigation aimed to discover the optimum heat treatment process under which the best dispersoid formation conditions with a large density and fine size can be achieved to maximize the elevated-temperature properties. After selecting the optimum heat treatment, all samples were subjected to the hot rolling at 400 ℃ followed by the post-rolling annealing at 500 ℃. The recrystallization behavior after hot rolling and during post-rolling annealing was further studied.

2. Experimental

Three Al-Mg-Si 6082 alloys with different Mn contents were prepared in the present study. The chemical compositions of the experimental alloys are listed in Table 1. Approximately 3 kg of materials for each alloy was melted in an electrical resistance furnace and then cast in a permanent metal mold to obtain the rectangular ingots (30 mm × 40 mm × 80 mm).

Cast ingots were subjected to various heat treatments ranging from 300 to 500 ℃ for up to 24 h with a heating rate of 100 ℃/h followed by water quenching. To evaluate the evolution of the dispersoids during the heat treatments and their influence on the mechanical properties at room temperature (RT) and elevated temperature, electrical conductivity (EC), Vickers microhardness and compression yield strength measurements were conducted. The EC was measured using a Sigmascope SMP10 electrical conductivity unit at RT, and the average value of 3 measurements was recorded for each condition. Microhardness tests were performed on an NG-1000 CCD

microhardness test machine with a load of 10 g and a dwell time of 20 s on polished samples. The indentations were applied inside the dendrite cells to evaluate the strengthening effect of dispersoids in the aluminum matrix, and the average value was obtained from 15 measurements for each sample. The elevated-temperature YS was obtained from compression tests performed on a Gleeble 3800 thermomechanical testing unit at 300 ℃ with a total strain of 0.2 and a fixed strain rate at 10^{-3} s^{-1}. A cylindrical specimen with dimensions of 15 mm in length and 10 mm in diameter was used. Prior to the compression tests, the specimens were annealed at 300 ℃ for 100 h to stabilize the microstructure.

For hot rolling tests, ingot samples were cut into a size of 30 mm × 40 mm × 40 mm and subjected to an optimum heat treatment (400 ℃/2 h) for the dispersoid precipitation. Before rolling, all samples were preheated to 400 ℃ for 30 minutes and then hot-rolled at 400 ℃ for several passes until reaching a final thickness of 3 mm from the original 30 mm. The reduction in thickness was controlled at 3 mm for each pass. After a few passes of rolling, the samples were returned to the furnace for reheating at 400 ℃ for 30 minutes to keep the rolling at a similar temperature. Then, the as-rolled samples were annealed at 500 ℃ for up to 8 h followed by water quenching.

To characterize the microstructure after rolling and annealing, all samples were sectioned and polished parallel to the rolling direction. The grain structure was analyzed using the electron backscattered diffraction (EBSD) technique with scanning electron microscopy (SEM, JOEL JSM-6480LV). Three different areas of 0.24 mm^2 for each condition were scanned with a step size of 2 μm. The evolution of the dispersoids formed during various heat treatments was characterized using optical microscopy (OM), SEM and transmission electron microscopy (TEM, JEOL JEM-2100). To clearly reveal the dispersoids, the polished samples were etched with 0.5% HF for 30 s for the OM and SEM observations.

3. Results and discussion

3.1 Microstructure in the as-cast and heat-treated conditions

The microstructures of the experimental alloys in the as-cast and heat-treated conditions were fully studied in the present work. As an example, the microstructures of Alloys A and C are shown in Fig. 1 to illustrate their evolution with the Mn addition. Figs. 1a-1b show that the as-cast

microstructures of Alloys A and C are similar, consisting of α-Al dendrites, dark primary Mg_2Si and gray Fe-rich intermetallics [19]. Based on the results of the image analysis, the volume fractions of primary Mg_2Si and Fe-rich intermetallics in Alloys A and C were 0.35 vol.% and 0.47 vol.% for Mg_2Si and 1.01 vol.% and 1.23 vol.% for the Fe-rich intermetallics, respectively. The Fe-rich intermetallics in Alloy C contained a small amount of Mn to replace Fe, and the increase in the volume fraction of Fe-rich intermetallics is not significant compared to that in Alloy A. Therefore, it suggests that most of Mn in Alloy C remained in the supersaturated solid solution of the aluminum matrix during solidification. This was further confirmed by the higher microhardness and lower EC of Alloy C in the as-cast condition, which was 69.1 HV and 28.9%IACS compared with 62.5 HV and 37.7%IACS for Alloy A.

Figs. 1c-1g shows the microstructures of Alloys A and C after heat treatment at 450 ℃/24 h. For both alloys, some of the primary Mg_2Si is dissolved during heat treatment, while little change in the Fe-rich intermetallics is observed. However, a significant difference can be observed in the aluminum matrix between the two alloys. As shown in Figs. 1c-1d for Alloy A, no dispersoids can form without Mn addition and only sparely coarsen Mg_2Si, which is likely formed during the heating and holding process, is distributed in the matrix. However, a large amount of dispersoids formed in Alloy C (Fig. 1e-1j). The dispersoid zone (indicated by blue circles) and dispersoid-free zone (DFZ, indicated by red circles) can be observed in the etched optical image (Fig. 1e). The details of the dispersoids are shown in the SEM (Fig. 1f) and TEM (Fig. 1g) images. The dispersoids in Fig. 1g are confirmed as Mn-containing α-Al(MnFe)Si dispersoids by the TEM-EDS results (results not shown here) and the data from the literature [5,12]. It is noteworthy that the characterization of the dispersoids by SEM and TEM is comparable. For instance, the average size of the dispersoids after 450 ℃/24 h is 112 nm from the SEM images while they are 96 nm from the TEM images, and the number density of dispersoids in both cases is similar. Since limited observations were performed with TEM, the evolution of the dispersoids for two Mn-containing alloys during heat treatment is based on the SEM characterization in the following section.

3.2 Evolution of dispersoids during heat treatment with various Mn contents

As shown in Fig. 1, a remarkable difference in the microstructure between Alloys A and C is observed after 450 ℃/24 h because of the precipitation of a high number of dispersoids in the

Mn-containing Alloy C due to the decomposition of supersaturated Mn in the aluminum matrix during heat treatment [5]. It is reported that the supersaturated solid solution level of Mn in the matrix can be indicated by the change in the EC according to the following equations [5, 12]:

$$1/EC_{Alloy\ A} = 0.0267 + 0.032\ Fe_{ss}\% + 0.0068Si_{ss}\% + 0.003Mg_{ss}\% \quad (1)$$

$$1/EC_{Alloy\ B/C} = 0.0267 + 0.032\ Fe_{ss}\% + \mathbf{0.033Mn_{ss}\%} + 0.0068Si_{ss}\% + 0.003Mg_{ss}\% \quad (2)$$

where Fe_{ss}%, Mn_{ss}%, Si_{ss}% and Mg_{ss}% are the weight percentages of the solute elements Fe, Mn, Si and Mg, respectively. Si_{ss} and Mg_{ss} have a much weaker effect on the EC than Mn_{ss} and Fe_{ss}, and most of Fe was in the form of intermetallics during solidification, such as Al_6(FeMn) and α-Al(MnFe)Si [2]. Therefore, the change in the EC difference between Alloy B/C and Alloy A can be used to estimate the evolution of the solid solution concentration of Mn in Alloy B/C during heat treatment by Eq. 3:

$$\Delta\rho = 1/EC_{Alloy\ B/C} - 1/EC_{Alloy\ A} = 0.033Mn_{ss}\% \quad (3)$$

Fig. 2 shows the differences in 1/EC (Δρ) between Alloy B/C and Alloy A during the heat treatments at various temperatures. Although the values of Δρ are different, a similar tendency of Δρ was found between Alloy B and Alloy A (Fig. 2a) and between Alloy C and Alloy A (Fig. 2b). When heat treated at 300 ℃, Δρ was high but stable over the soaking time, indicating that most of the Mn atoms are still remaining in the aluminum matrix in Alloys B and C. At 350 ℃, Δρ decreased sharply with increasing soaking time, indicating a continuous decrease in the Mn solute concentration in the matrix and the formation of dispersoids. Variations of Δρ at 400 ℃ and 450 ℃ were similar, which exhibited an initial fast drop followed by a plateau after 4-8 h holding, indicating the full decomposition of the Mn supersaturated solid solution. The Δρ at 500 ℃ showed the lowest value among the given heat treatment conditions and paralleled with the plateau achieved at 400 ℃ and 450 ℃, suggesting that decomposition of the Mn solutes in the solid solution was complete even before 1 h at 500 ℃.

The corresponding difference in Vickers microhardness (ΔHV) between Alloy B/C and Alloy A in the temperature range of 350-500 ℃ is shown in Fig. 3. The hardness curves in Fig. 3 can be regrouped into two types: Type I is in the temperature range of 350-400 ℃, where ΔHV continues to increase until reaching a plateau; Type II is in the temperature range of 450-500 ℃, where the ΔHV begins to decrease after reaching the peak value. As shown in Fig. 3a and 3b, ΔHV at 350 ℃ in Alloys B and C increases gradually up to 24 h, indicating the start of the dispersoid precipitation

at that temperature (see also Fig. S1 in the supplementary materials), while ΔHV reaches the highest value at 400 ℃ after 2 h due to the almost complete precipitation of dispersoids, which is 20 HV for ΔHV_{B-A} and 25 HV for $\Delta HV_{C-A.}$ Since the change in the hardness is mainly related to the formation of dispersoids, the evolution of dispersoids during the heat treatment at 400 ℃ (Type I) and 500 ℃ (Type II) was selected for the detailed discussion in the following section. As a reference, the microhardness of Alloy A as a function of soaking time is shown in Fig. 3c to show the hardness value of the experimental alloys during various heat treatments. The microhardness of Alloy A decreases with soaking time when the temperature is lower than 450 ℃ due to the precipitation of coarsen Mg_2Si precipitates out of the matrix (Fig. 1 d), while it increases with the soaking time when treated at 500 ℃ due to the dissolution of Mg_2Si precipitates back into the matrix [20].

Fig. 4 shows the evolution of dispersoids during the heat treatment at 400 ℃. In Alloy A, no dispersoids could be observed after 24 h but only a few coarsened Mg_2Si precipitates (Fig. 4a). However, in Alloy B (Figs. 4b-4d) and Alloy C (Figs. 4e-4g), fine dispersoids were already uniformly distributed in the matrix after 1 h holding and remained stable after 24 h of soaking (Figs. 4d and 4g). The image analysis results (Fig. 5) show that the number density of the dispersoids initially increases in the first 2 h and then remains steady, while the size of the dispersoids increases in the first 4 h and is almost constant up to 24 h with an average diameter of 74 nm in Alloy B and 85 nm in Alloy C. The above results indicate that the dispersoids started to precipitate shortly after reaching 400 ℃ and reached the optimum and stable condition after 2-4 h. In fact, as shown in Figs. 2 and 3, the dispersoids could precipitate at low temperatures, such as starting from 350 ℃. By comparing Alloy B and Alloy C, a denser distribution of dispersoids is observed in Alloy C with a high Mn content. The number density of dispersoids after 400 ℃/24 h increases from ~9 μm^{-2} in Alloy B to 13 μm^{-2} in Alloy C, while the equivalent diameter increases moderately from 74 nm in Alloy B to 85 nm in Alloy C.

Figs. 6 and 7 present the evolution of dispersoids in Alloys B and C at 500 ℃. Compared to the condition treated at 400 ℃ (Figs. 4 and 5), it is apparent that the size of the dispersoids at 500 ℃ was much larger. In addition, the number density of the dispersoids decreases and the size increases with the soaking time, indicating that the coarsening of the dispersoids dominated over time at 500 ℃, leading to the lowest ΔHV at 500 ℃ for both Alloy B and Alloy C (Fig. 3). As shown in Figs. 6 and 7 at 500 ℃/1 h, the initial size of the dispersoids in Alloys B and C is not largely

different, but the number density in Alloy C is higher. However, after 2 h, the dispersoids became coarsening, and the dispersoid coarsening was faster in Alloy C because the number density of the dispersoids decreases more sharply and the size increases faster in Alloy C than in Alloy B (Figs. 6 and 7). Upon further increasing the time to 24 hours, a large difference can be observed in terms of the number density and size of the dispersoids, confirming the higher coarsening rate of dispersoids in Alloy C. In addition, the evolution of dispersoids at 450 ℃ is shown in Fig. S2 as the supplementary materials. In connection with the changes in the EC (Fig. 2) and HV (Fig. 3), it is evident that the coarsening of the dispersoids occurred starting from 450 ℃.

The influence of the heat treatment temperature and Mn content on the dispersoids can be attributed to the rapid increase in the diffusion rate of Mn with increasing temperature and Mn concentration. At relatively low temperatures (350-400 ℃), the diffusion of Mn solutes is limited to a short distance, and thus, the growth of the dispersoids is restricted [21]. However, at high temperatures (450-500 ℃), long-distance diffusion of Mn solutes is possible, and the growth and coarsening of dispersoids is promoted [21, 22]. On the other hand, the addition of higher Mn in Alloy C increases the concentration gradient at the interface of the dispersoids, and its influence on the diffusion rate is mitigated by a smaller diffusion coefficient at low temperatures but amplified by a larger diffusion coefficient at high temperatures, leading to the faster coarsening of dispersoids in Alloy C than Alloy B [21, 22].

3.3 Elevated-temperature strength and thermal stability of dispersoids

As shown in Figs. 4-7, different precipitation behaviors of the dispersoids in Alloys B and C can be observed, including the changes in the number density and size with the heat treatment temperature and time. Therefore, a few typical heat treatment conditions, such as the initial precipitation stage (350 ℃/24 h), the peak precipitation condition (400 ℃/2 h), the stable precipitation stage (450 ℃/2 h) and the coarsening stage (450 ℃/16 h), were selected to investigate the effect of dispersoids on the YS at elevated temperature (300 ℃). To stabilize the microstructure, all samples were held at 300 ℃ for 100 h prior to mechanical testing. The results are shown in Fig. 8. The YS of the base alloys (Alloy A) varied between 23 and 30 MPa depending on the heat treatment conditions. A significant improvement in YS in the Mn-dispersoid-containing Alloys B and C is observed compared with the base alloy under all given heat treatment conditions. For Alloy

B (0.5% Mn), the highest value of YS is 55 MPa at 400 ℃/2 h and 450 ℃/2 h. For Alloy C (1%Mn), the highest YS is 70 MPa under 350 ℃/24 h and 400 ℃/2 h conditions compared to 30 and 28 MPa for Alloy A under such conditions, which represents a more than 130% improvement in the YS at 300 ℃, confirming the essential contribution of the precipitation of dispersoids on the elevated-temperature strength [14]. With the increasing heat treatment temperature, a gradual decrease in YS is observed for Alloy C at 450 ℃/2 h and 450 ℃/16 h, whereas the YS of Alloy B decreases slightly at 450 ℃/16 h due to the coarsening of dispersoids at high temperature [5, 23]. On the other hand, the difference in YS between Alloy B and Alloy C also changes with the precipitation treatment conditions. At the peak condition of 400 ℃/2 h, the YS difference between Alloy B and Alloy C is 15 MPa due to the higher number density of dispersoids but with a similar size in Alloy C (Fig. 4c, 4f and Fig. 5). However, the difference in YS between Alloy B and Alloy C decreases to 4 MPa at 450 ℃/16 h due to the higher coarsening rate of dispersoids in Alloy C (Fig. 3 and Fig. 2S).

For the precipitate-strengthened aluminum alloys, the room-temperature strength can be well explained by the classical Orowan bypass mechanism for the large precipitate size. . Approaches have been made to estimate the strengthening effect of dispersoids at elevated temperatures using Orowan mechanism [24-26], but it is still too far to provide satisfactorily quantitative results. The strengthening mechanisms at elevated temperature are more complex than the room temperature because there is sufficient thermal energy to allow more activities happen, such as the higher vacancy and solute diffusion, higher grain boundary movement and the activation of multi-slip systems for dislocations, etc. Therefore, only the experimental evidences of the improvement on elevated-temperature strength from dispersoids is presented here. To better understand the strengthening mechanisms at high temperature and to quantify the elevated-temperature strength induced by thermally stable dipsersoids is subject of our ongoing investigation."

After the peak precipitation condition (400 ℃/2 h) to obtain the maximum strength (Fig. 8), a long-term thermal exposure at 300 ℃ for up to 1000 h was performed for Alloy C to assess the thermal stability of the dispersoids. Fig. 9 displays the evolution of the microhardness and dispersoids during long-term thermal holding. The microhardness remains fairly constant between 68-71 HV (Fig. 9a), and the number density and size of dispersoids hardly change during the 1000 h thermal holding (Fig. 9b-d). This result confirms that the α-Al(MnFe)Si dispersoids in 6082 alloys

have excellent thermal stability at 300 °C, which can be attributed to 1) the relative high precipitation temperature (around 350-400 °C, mentioned in the section 3.1), and 2) α-Al(MnFe)Si dispersoids precipitated from the supersaturated solid solution are the stable phase and partially coherent with aluminum matrix [27]. The results are consistent with those obtained. The results are consistent with those obtained in dispersoid-containing 3xxx [5, 28].

3.4 Recrystallization behaviors during hot rolling and post-rolling annealing

Prior to rolling, ingot samples were subjected to a heat treatment at 400 ℃/2 h to reach the peak condition for dispersoid precipitation (Fig. 4). The rolling was performed at 400 ℃, and Fig. 10 shows the as-rolled microstructure of the experimental alloys. It can be found that the grain structure in Alloy A is almost equiaxed, and some grains are slightly elongated in the rolling direction (Fig. 10a), indicating partial or full recrystallization during the rolling process. Dislocation bands and subgrain boundaries can still be observed in the more and less equiaxed grains, which were likely formed by the last rolling passes. According to the microstructure in Fig. 10a, it is reasonable to make the assumption that at least the partial recrystallization occurred during each pass of the rolling and between the reheating processes. Alloy A had only some coarse Mg_2Si particles but was free of dispersoids (Fig. 4a) and therefore, it exhibited almost no retarding effect on recrystallization during hot rolling [29]. On the other hand, the grain structure in Alloys B and C is a typical deformed and recovery structure consisting of deformed bands and highly elongated grains paralleling to the rolling direction with a very small amount of fine recrystallized grains. As described in Section 3.2, a large amount of fine dispersoids precipitated after the heat treatment at 400 ℃/2 h prior to rolling (Figs. 4c and 4f). These dispersoids are thermally stable at 400 ℃ (Figs. 4d and 4g) and play a significant role in retarding recrystallization during hot rolling, resulting in the elongated and deformed grain structure remaining in Alloys B and C [3, 30, 31].

After hot rolling, the samples were annealed at 500 ℃ for up to 8 h, and Fig. 11 shows the evolution of the microstructure of the experimental alloys during the post-rolling annealing. For Alloy A, a recrystallized microstructure is almost achieved after 1 hour (Fig. 11a), although a few subgrains remain in some gains. The completion of recrystallization occurs after 2 h (Fig. 11d). With increasing annealing time, the grains slightly grow, and the equiaxed grains remain almost unchanged up to 8 h (Fig. 11g). On the other hand, no obvious recrystallization can be observed in

Alloy B even up to 8 h. As shown in Figs. 11b and 11e, the highly elongated grains are the main characteristic of the microstructure after 1-2 h annealing. With increasing time, the number of subgrains decreases, and the recovery is in progress. As shown in Fig. 11h after 500 ℃/8 h, the microstructure of Alloy B still exhibits a main recovery grain structure with a small amount of fine and isolated recrystallized grains on the grain boundaries (indicated by the red circle), indicating the excellent recrystallization resistance of Alloy B. For Alloy C, it shows a partially recrystallized microstructure after 1-2 h (Figs. 11c and 11f), presenting as some fine recrystallized grains that nucleated and grew heterogeneously on the grain boundaries between elongated gains (see the white circle in Figs. 11c and f). However, the number of newly recrystallized grains increases only slightly with time; therefore, the elongated recovery grains are still dominant in the microstructure up to 8 h (Fig. 11i), indicating the good recrystallization resistance of Alloy C, which is much better than that of Alloy A but less than that of Alloy B.

Generally, the recrystallization process is initiated from the formation of strain-free subgrains followed by the subsequent growth into recrystallized grains at the expense of the surrounding deformed matrix. The results in Figs. 10 and 11 reveal that the formation of dispersoids prior to rolling is of particular importance to control the recrystallization behavior during hot rolling and post-rolling annealing. The effectiveness of dispersoids in preventing recrystallization can be commonly expressed by using the Zener drag P_Z that provides a back-driving pressure on the moving grain boundary, which can be calculated in the following equation [31, 32]:

$$P_z = \frac{3\gamma_{GB}F_v}{D} \quad (4)$$

where γ_{GB} is the specific grain boundary energy, F_V and D are the volume fraction and average diameter of dispersoids, respectively. As indicated in Eq. 4, a high amount of dispersoids (i.e., a high F_V/D value) is essential to achieve a high P_Z on grain boundary migration for retarding the growth of recrystallized grains. As mentioned above, Alloy A had only a few coarse Mg_2Si particles in the aluminum matrix and was free of dispersoids; therefore, the *Pz* is very small, resulting in a poor recrystallization resistance. After the heat treatment at 400℃/2 h prior to rolling, a large number of dispersoids were present in Alloys B and C, and then P_Z increases significantly, leading to much higher recrystallization resistance than Alloy A. However, Alloy B had a lower number density of dispersoids but their size was smaller compared to Alloy C (Fig. 5). The opposite effect of the number density and size of the dispersoids in Alloys B and C might lead to a similar *Pz* and

thus result in a similar recrystallization resistance after hot rolling (Figs. 10b and 10c)

The general tendency of the recrystallization behaviors of the three alloys during post-rolling annealing is similar to that during hot rolling; e.g., the recrystallization resistance of both Mn-dispersoid-containing alloys (B and C) is much better than that of the Alloy A free of dispersoids. However, the recrystallization resistance of Alloy C is less than that of Alloy B (Fig. 11), presenting as a higher amount of fine recrystallized grains during post-rolling annealing. This difference might be attributed to the higher coarsening rate of dispersoids in Alloy C at a high holding temperature (500 ℃) than that in Alloy B (Fig. 7). Meanwhile, a higher volume fraction of intermetallic particles and the larger dispersoid free zone C is observed in Alloy due to its high amount of Mn content in our previous study [33], which would likely contribute to more available nucleation sites for recrystallization, leading to a relatively lower recrystallization resistance compared to Alloy B. However, the exact reasoning is not clear at the moment and needs to be further studied.

4. Conclusions

(1) With Mn additions (0.5-1.0%) to Al-Mg-Si 6082 alloys, α-Al(MnFe)Si dispersoids began to precipitate at 350 ℃ and reached the optimum conditions at 400 ℃ for 2-4 hours with a high number density (10-15 μm^{-2}) and fine size (70-80 nm). However, the dispersoids became coarse with increasing holding time at temperatures above 450 ℃.

(2) After the peak precipitation treatment at 400 ℃ for 2 h, the precipitation of a large amount of dispersoids greatly enhanced the elevated-temperature strength. The yield strength at 300 ℃ increased from 28 MPa (the base alloy free of Mn) to 55 MPa (the alloy containing 0.5% Mn) and 70 MPa (the alloy containing 1% Mn), respectively.

(3) During a long-term thermal exposure at 300 ℃, α-Al(MnFe)Si dispersoids in 6082 alloys are thermally stable up to 1000 h owing to its relative high precipitation temperature, resulting in the superior constant mechanical performance during the long service life at elevated temperature.

(4) During hot rolling and post-rolling annealing, the presence of a large amount of dispersoids significantly increase the Zener drag P_Z and therefore improved the recrystallization resistance. In the as-rolled condition, a high volume of recrystallized grains was observed in the base alloy, but it was dominated by highly elongated grains in the Mn-containing alloys. During post-rolling

annealing at 500 °C, a full recrystallized structure was reached only after 1 h in the base alloy, whereas the main recovery grain structure remained up to 8 h in the Mn-containing alloys.

(5) Under the same post-rolling annealing conditions, the alloy containing 0.5% Mn exhibited the highest recrystallization resistance among all three experimental alloys studied, likely benefitting from the lower coarsening rate of dispersoids and smaller fraction of dispersoids free zones.

Acknowledgements

The authors acknowledge the financial support of the Natural Sciences and Engineering Research Council of Canada (NSERC) and Rio Tinto Aluminum through the NSERC Industry Research Chair in the Metallurgy of Aluminum Transformation at the University of Quebec at Chicoutimi.

References

[1] J. Dutkiewicz, L. Litynska, Mater. Sci. Eng., A 324 (2002) 239-243.
[2] L.P. Troeger, E.A. Starke, Mater. Sci. Eng., A 277 (2000) 102-113.
[3] R. Hu, T. Ogura, H. Tezuka, T. Sato, Q. Liu, J. Mater. Sci. Technol. 26 (2010) 237-243.
[4] M. Usta, M.E. Glicksman, R.N. Wright, Metall. Mater. Trans. A 35 (2004) 435-438.
[5] K. Liu, X.G. Chen, Mater. Des. 84 (2015) 340-350.
[6] D. Tsivoulas, P.B. Prangnell, Acta Mater. 77 (2014) 1-16.
[7] S. Tangen, K. Sjølstad, T. Furu, E. Nes, Metall. Mater. Trans. A 41 (2010) 2970-2983.
[8] P. Mukhopadhyay, M. Loeck, G. Gottstein, Acta Mater. 55 (2007) 551-564.
[9] F. Hichem, G. Rebai, Appl. Phys. A 119 (2015) 285-289.
[10] R.A. Jeniski, B. Thanaboonsombut, T.H. Sanders, Metall. Mater. Trans. A 27 (1996) 19-27.
[11] E. Nes, N. Ryum, O. Hunderi, Acta Metall. 33 (1985) 11-22.
[12] K. Liu, X.-G. Chen, J. Mater. Res. 32 (2017) 2585-2593.
[13] K. Liu, X.G. Chen, Metall. Mater. Trans. B 47B (2015) 3291-3300.
[14] K. Liu, H. Ma, X.G. Chen, J. Alloys Compd. 694 (2017) 354-365.
[15] M. Somerday, F.J. Humphreys, Mater. Sci. Technol. 19 (2003) 20-29.
[16] I. Nikulin, A. Kipelova, S. Malopheyev, R. Kaibyshev, Acta Mater. 60 (2012) 487-497.
[17] B. Forbord, L. Auran, W. Lefebvre, H. Hallem, K. Marthinsen, Mater. Sci. Eng., A 424 (2006) 174-180.
[18] A.R. Eivani, H. Ahmed, J. Zhou, J. Duszczyk, Metall. Mater. Trans. A 40 (2009) 2435-2446.
[19] G. Mrówka-Nowotnik, J. Sieniawski, J. Mater. Process. Technol. 162-163 (2005) 367-372.
[20] A.R. Prabhukhot, IJAMSE 3 (2015) 287-294.
[21] A. Rodin, N. Goreslavets, Defect Diff. Forum 383 (2018) 31-35.
[22] N.N. Goreslavets, A.O. Rodin, Phys. Met. Metallogr. 118 (2017) 1120-1126.
[23] K. Liu, X.G. Chen, Mater. Sci. Eng. A 697 (2017) 141-148.

[24] G.S. Wang, K. Liu, S.L. Wang, Materials 11 (2018) 1158.
[25] Z. Li, Z. Zhang, X.G. Chen, Mater. Sci. Eng., A 729 (2018) 196-207.
[26] Z. Li, Z. Zhang, X.G. Chen, Mater. Sci. Eng., A 708 (2017) 383-394.
[27] Y.J. Li, A.M.F. Muggerud, A. Olsen, T. Furu, Acta Mater. 60 (2012) 1004-1014.
[28] K. Liu, H. Ma, X.G. Chen, Metall. Mater. Trans. B 49 (2018) 1588-1596.
[29] S. De La Chapelle, P. Duval, Texture Microstruct. 35 (2002) 55-70.
[30] C. Shi, X.G. Chen, Mater. Sci. Eng., A 613 (2014) 91-102.
[31] J. Lai, C. Shi, X.G. Chen, Mater. Charact. 96 (2014) 126-134.
[32] Z. Guo, G. Zhao, X.G. Chen, Mater. Charact. 102 (2015) 122-130.
[33] C. Li, K. Liu, N. Parson, X.-G. Chen, in: Proceeding of 16th international Aluminum Alloys Conference (ICAA16), Mcgill University, Montreal, Canada, June 17-21, 2018.

Figure and Table captions

Table 1 Chemical composition (wt.%) of the experimental alloys

Fig. 1 Microstructures of Alloys A and C in as-cast condition (a-b) and after heat treatment at 450 ℃/24h (c-g)

Fig. 2 Differences in 1/EC during the heat treatments at various temperatures: (a) between Alloy B and Alloy A and (b) between Alloy C and Alloy A

Fig. 3 Differences in Vickers hardness (ΔHV) during heat treatments between Alloy B and Alloy A (a), and between Alloy C and Alloy A (b); and (c) HV values of Alloy A as a function of soaking time

Fig. 4 Microstructure and evolution of dispersoids when treated at 400℃: (a) Alloy A; (b-d) Alloy B and (e-g) Alloy C

Fig. 5 Evolution of the number density (a) and equivalent diameter (b) of dispersoids when treated at 400 ℃

Fig. 6 Evolution of dispersoids after treated at 500 ℃: (a-c) Alloy B and (d-f) Alloy C

Fig. 7 Evolution of the number density (a) and equivalent diameter (b) of dispersoids when treated at 500 ℃

Fig. 8 Yield strength at 300 ℃ of experimental alloys at typical heat treatment conditions

Fig. 9 Evolution of the microhardness (a) and SEM images showing no remarkable changes of dispersoids during long-term thermal exposure (b-d)

Fig. 10 As-rolled microstructure of experimental alloys

Fig. 11 Evolution of microstructure during the post-rolling annealing of experimental alloys

Fig. S1 Distribution of dispersoids at 350 ℃in Alloys B and C

Fig. S2 Distribution of dispersoids at 450 ℃ in Alloys B and C

Table list:

Table 1 Chemical composition (wt.%) of the experimental alloys

Alloy	Fe	Mg	Si	Mn	Al
A	0.26	0.99	0.66	**0.00**	Bal.
B	0.27	1.07	0.67	**0.52**	Bal.
C	0.23	1.12	0.69	**1.06**	Bal.

Figure list:

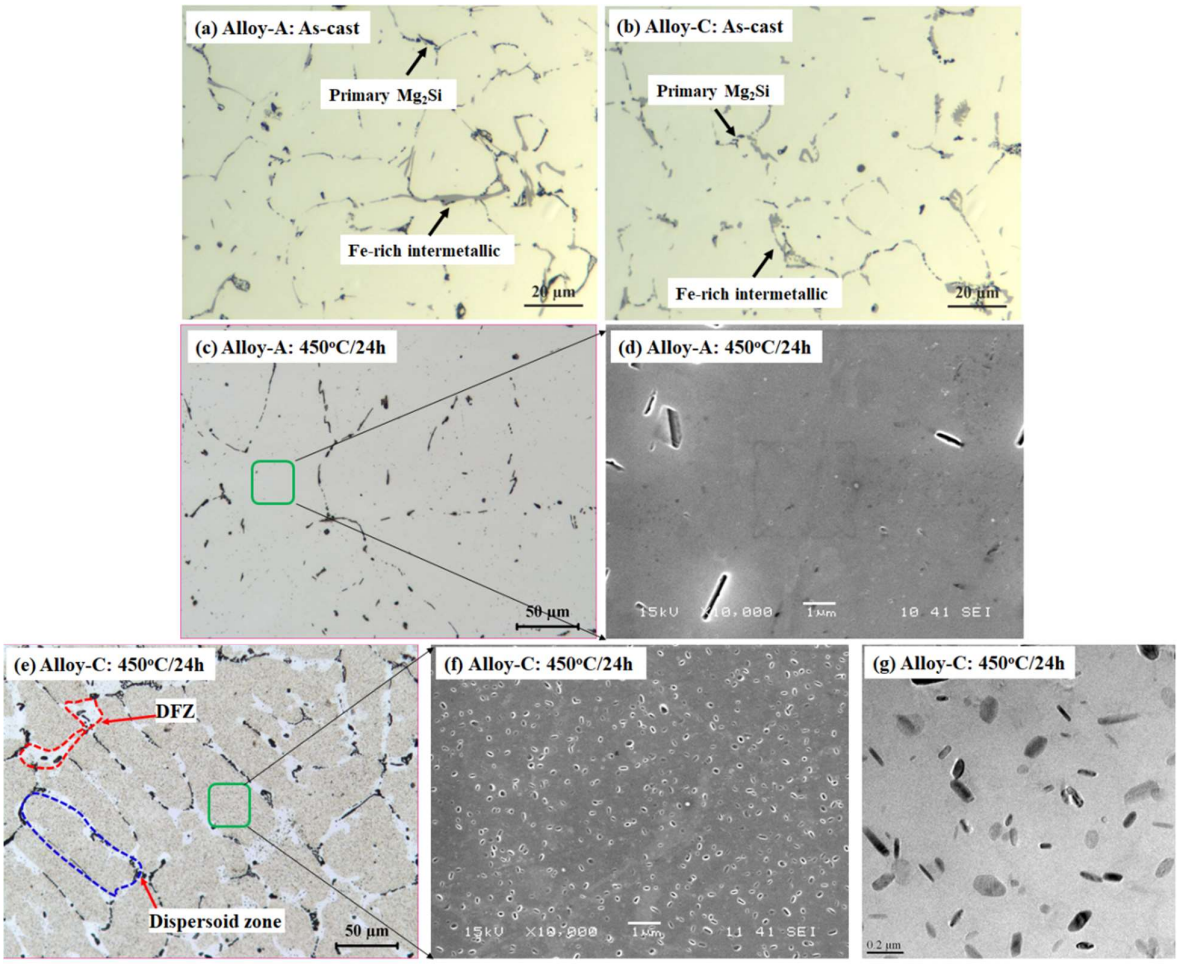

Fig. 1 Microstructures of Alloys A and C in as-cast condition (a-b) and after heat treatment at 450 ℃/24h (c-g)

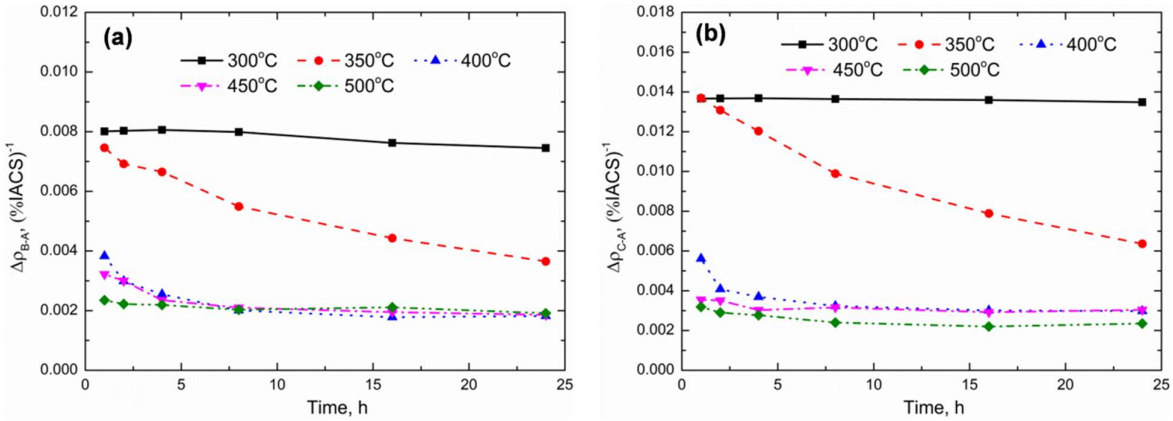

Fig. 2 Differences in 1/EC during the heat treatments at various temperatures: (a) between Alloy B and Alloy A and (b) between Alloy C and Alloy A

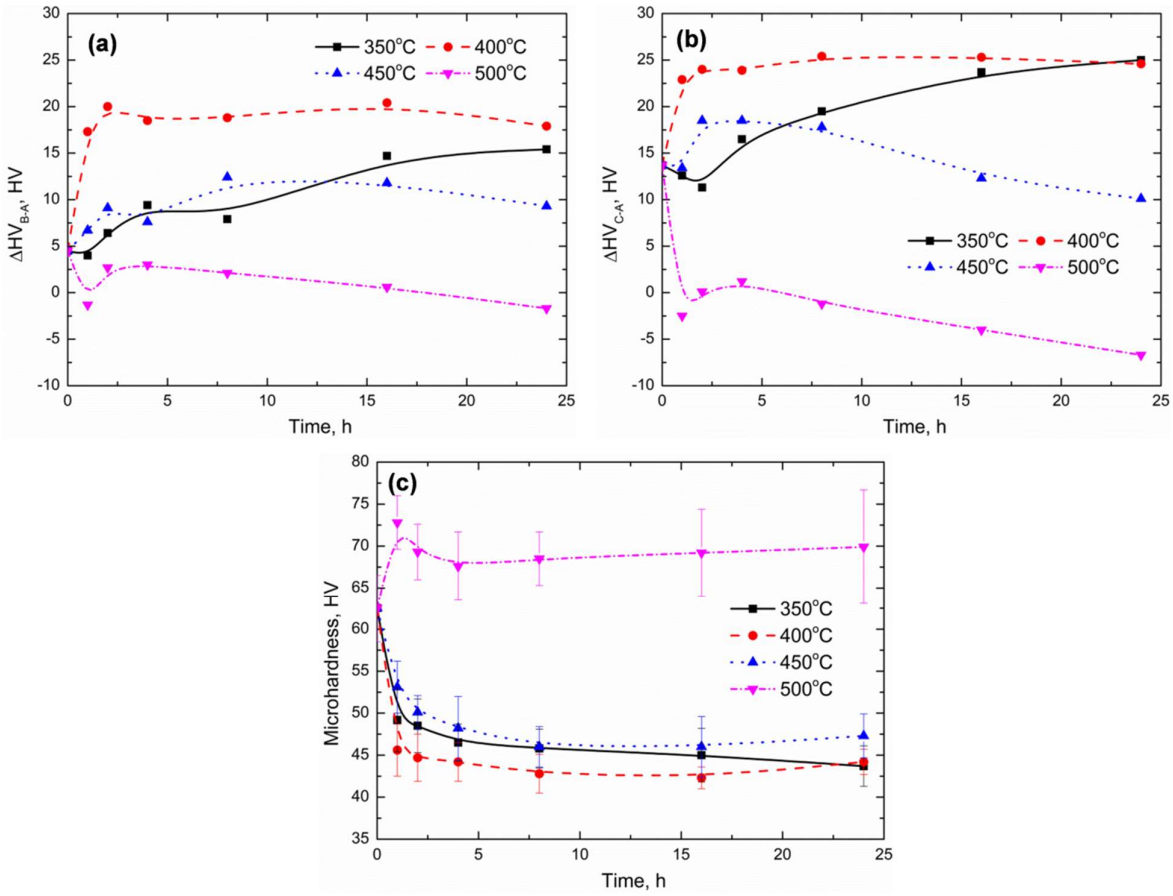

Fig. 3 Differences in Vickers hardness (ΔHV) during heat treatments between Alloy B and Alloy A (a), and between Alloy C and Alloy A (b); and (c) HV values of Alloy A as a function of soaking time

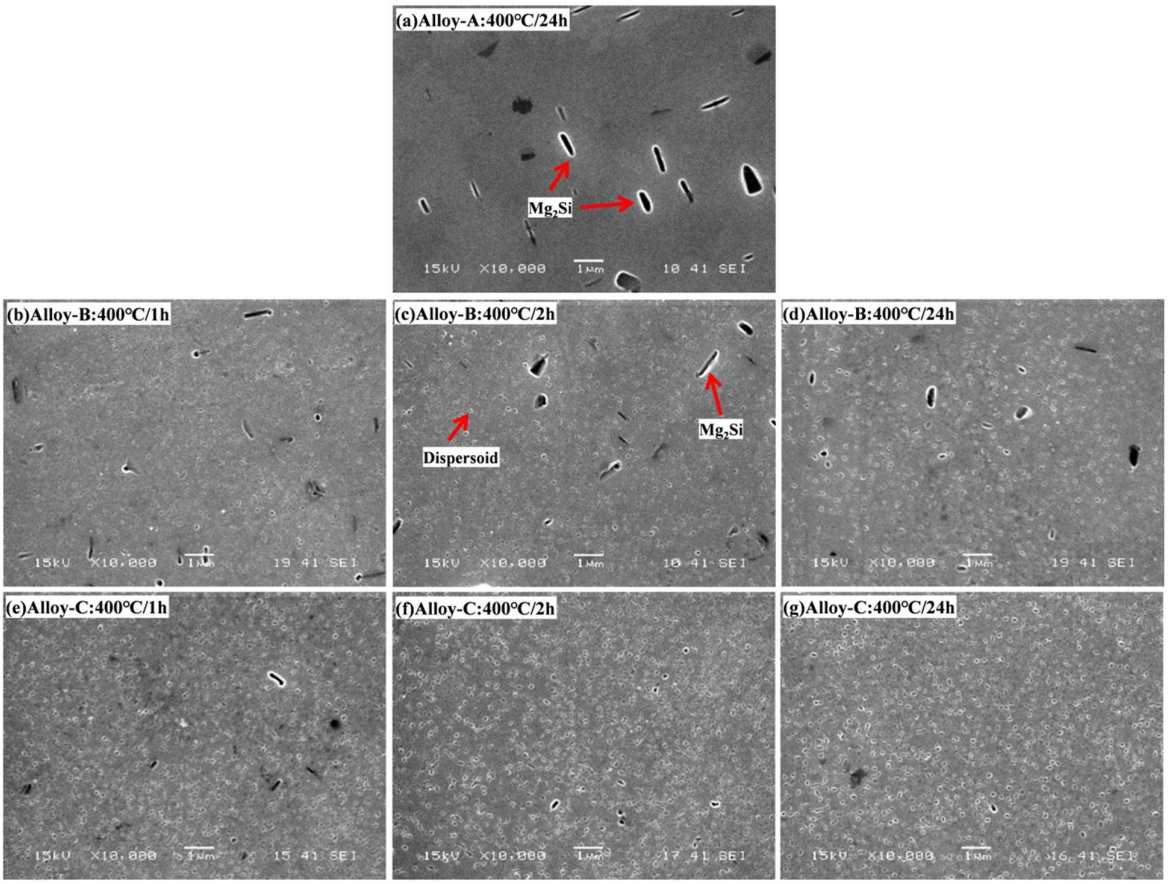

Fig. 4 Microstructure and evolution of dispersoids when treated at 400℃:

(a) Alloy A; (b-d) Alloy B and (e-g) Alloy C

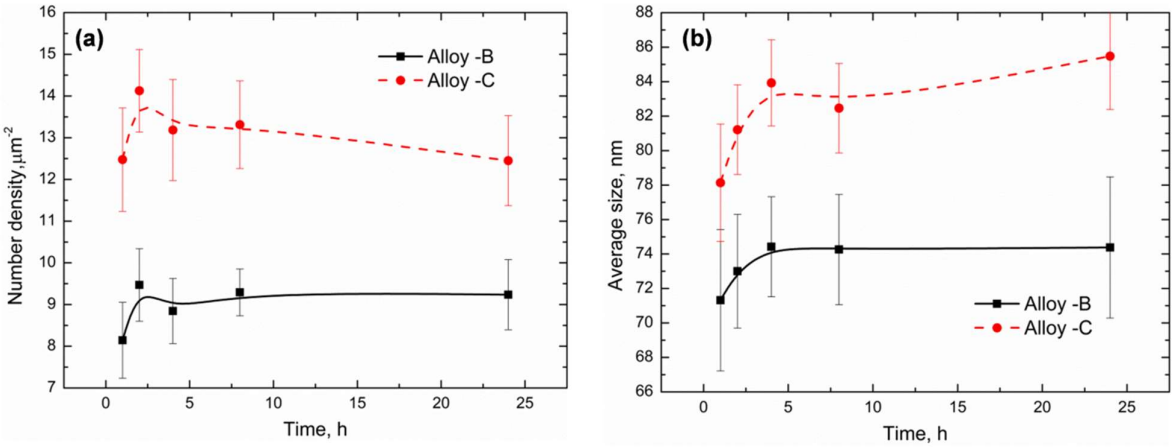

Fig. 5 Evolution of the number density (a) and equivalent diameter (b) of dispersoids when treated at 400 °C

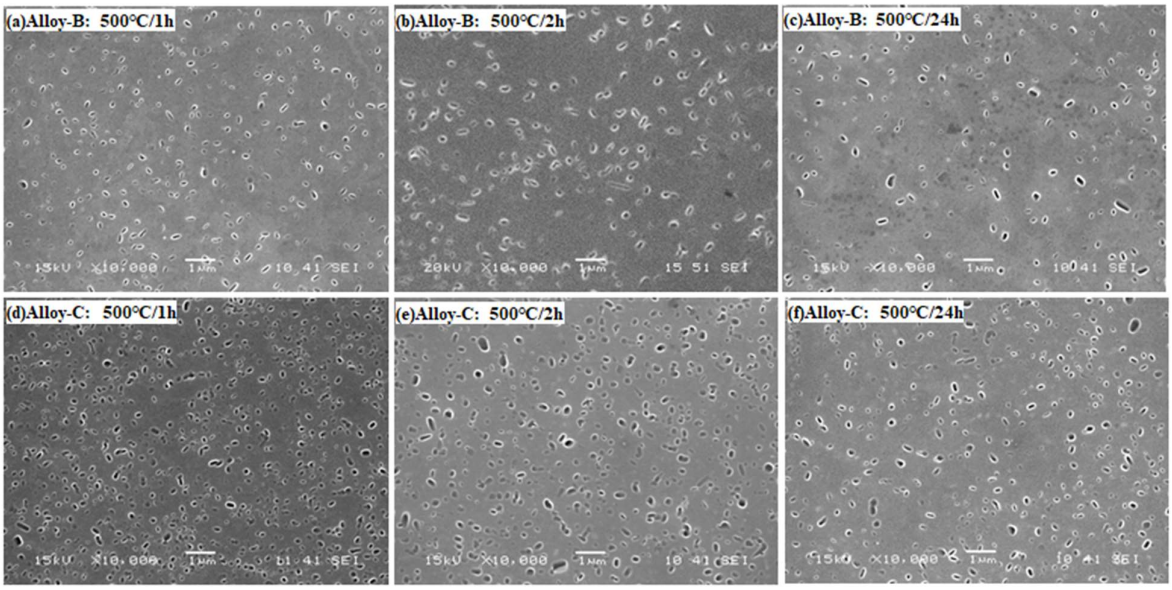

Fig. 6 Evolution of dispersoids after treated at 500 ℃: (a-c) Alloy B and (d-f) Alloy C

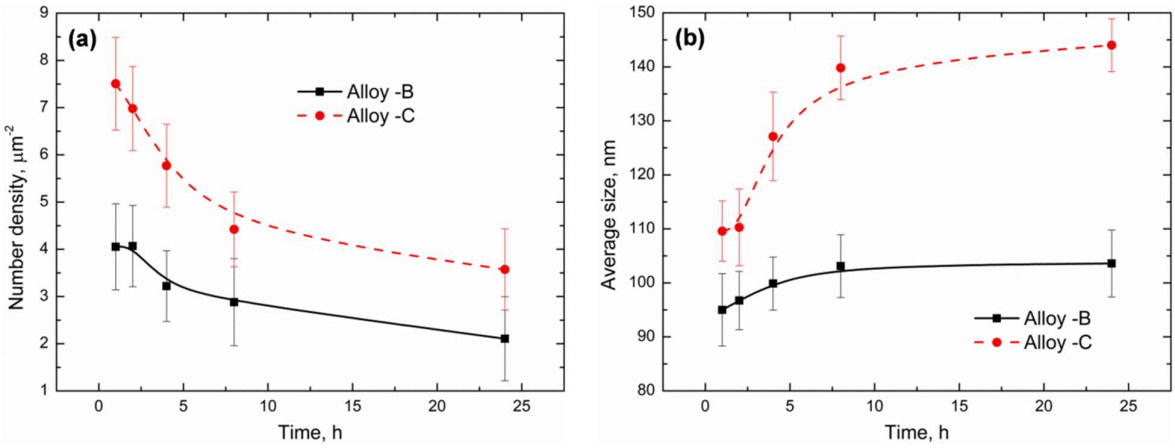

Fig. 7 Evolution of the number density (a) and equivalent diameter (b) of dispersoids when treated at 500 ℃

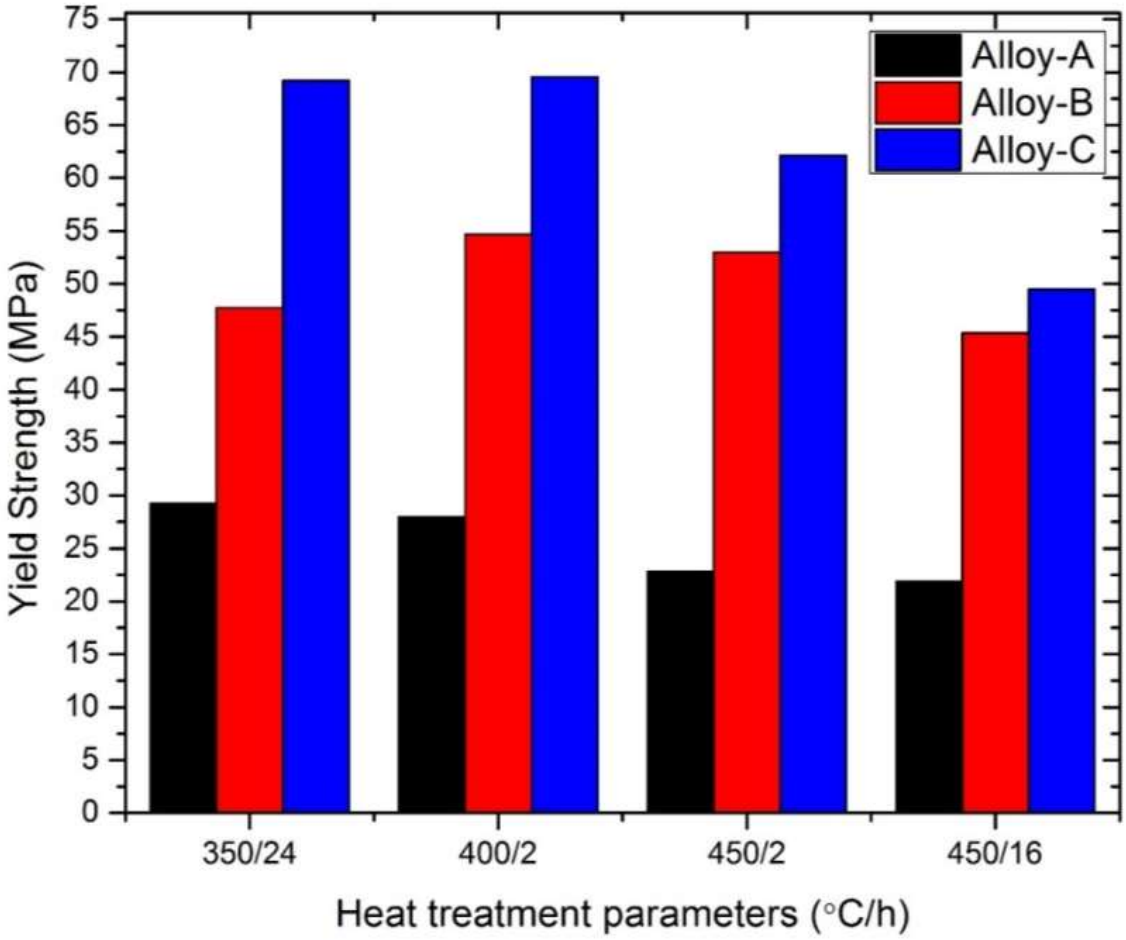

Fig. 8 Yield strength at 300 ℃ of experimental alloys at typical heat treatment conditions

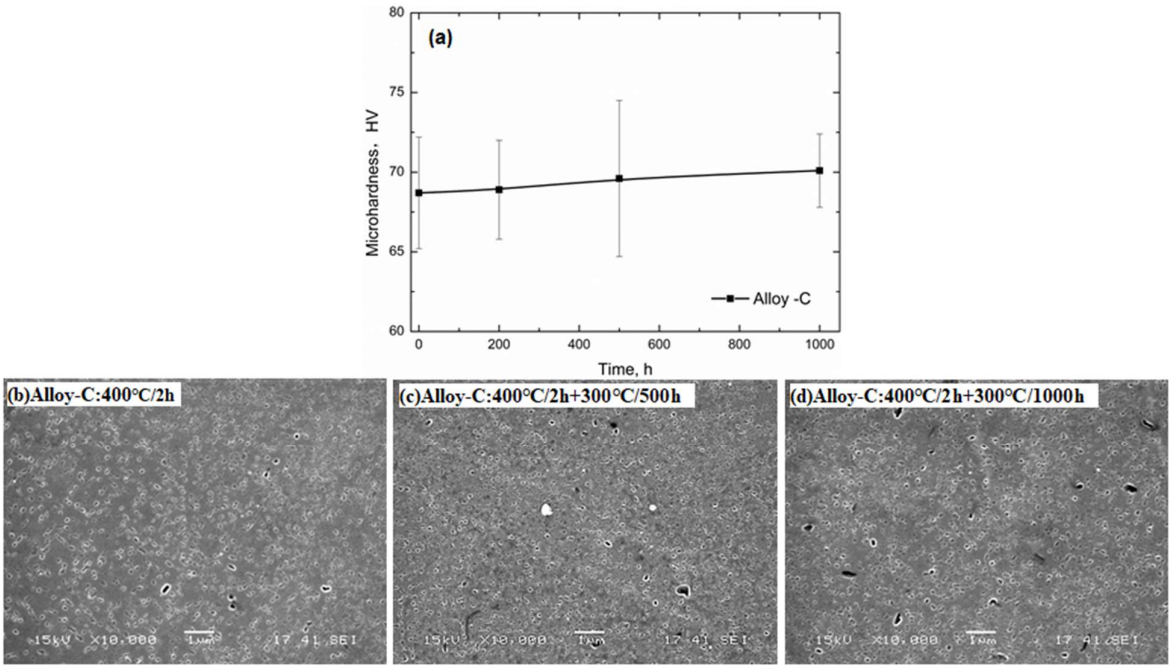

Fig. 9 Evolution of the microhardness (a) and SEM images showing no remarkable changes of dispersoids during long-term thermal exposure (b-d)

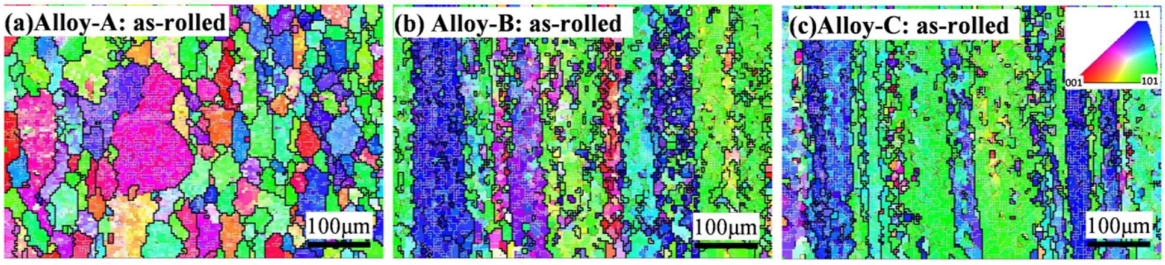

Fig. 10 As-rolled microstructure of experimental alloys

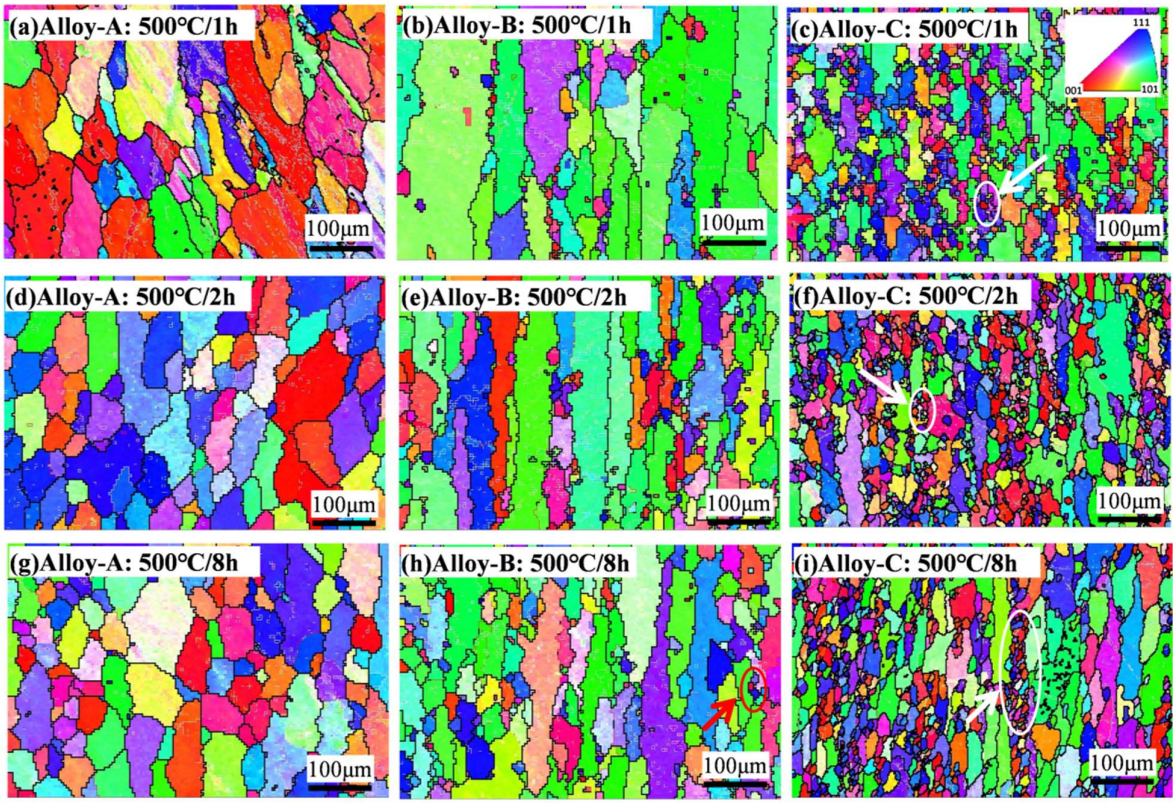

Fig. 11 Evolution of microstructure during the post-rolling annealing of experimental alloys

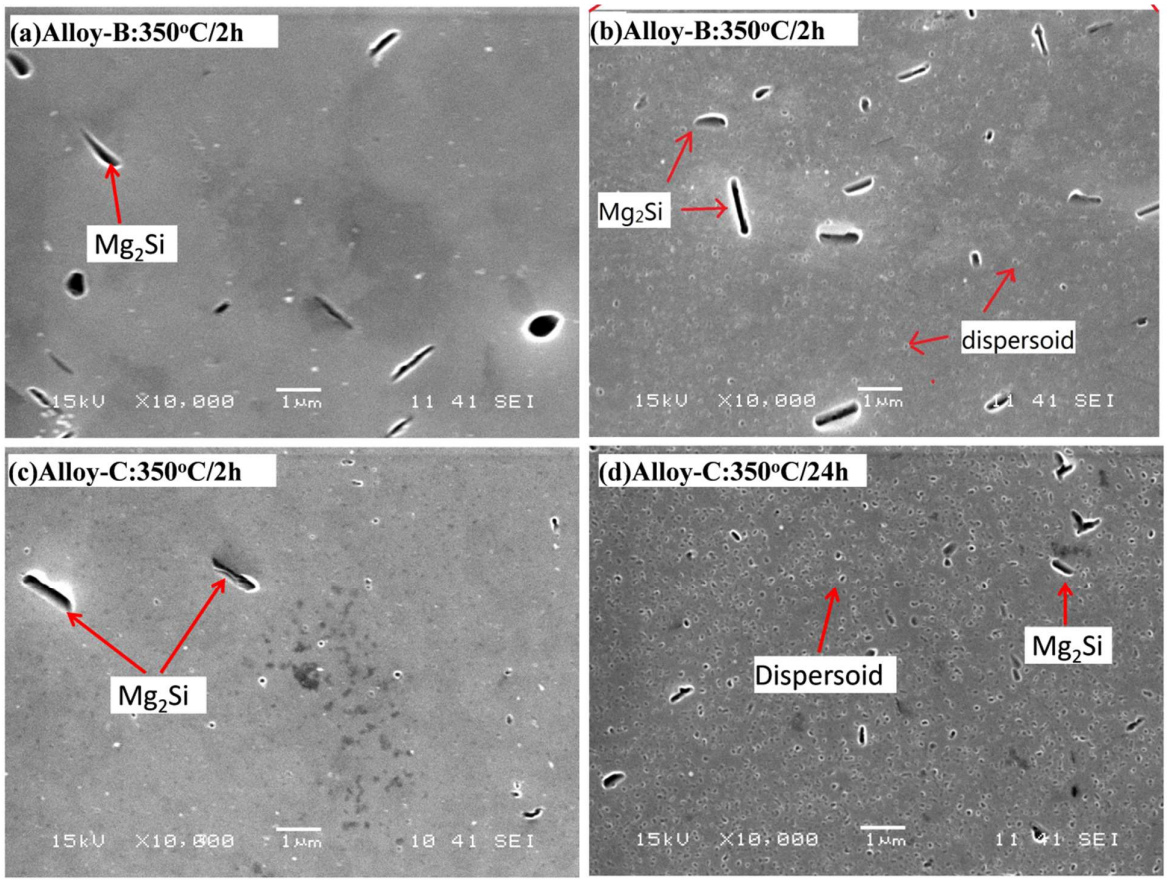

Fig. S1 Distribution of dispersoids at 350 ℃ in Alloys B and C

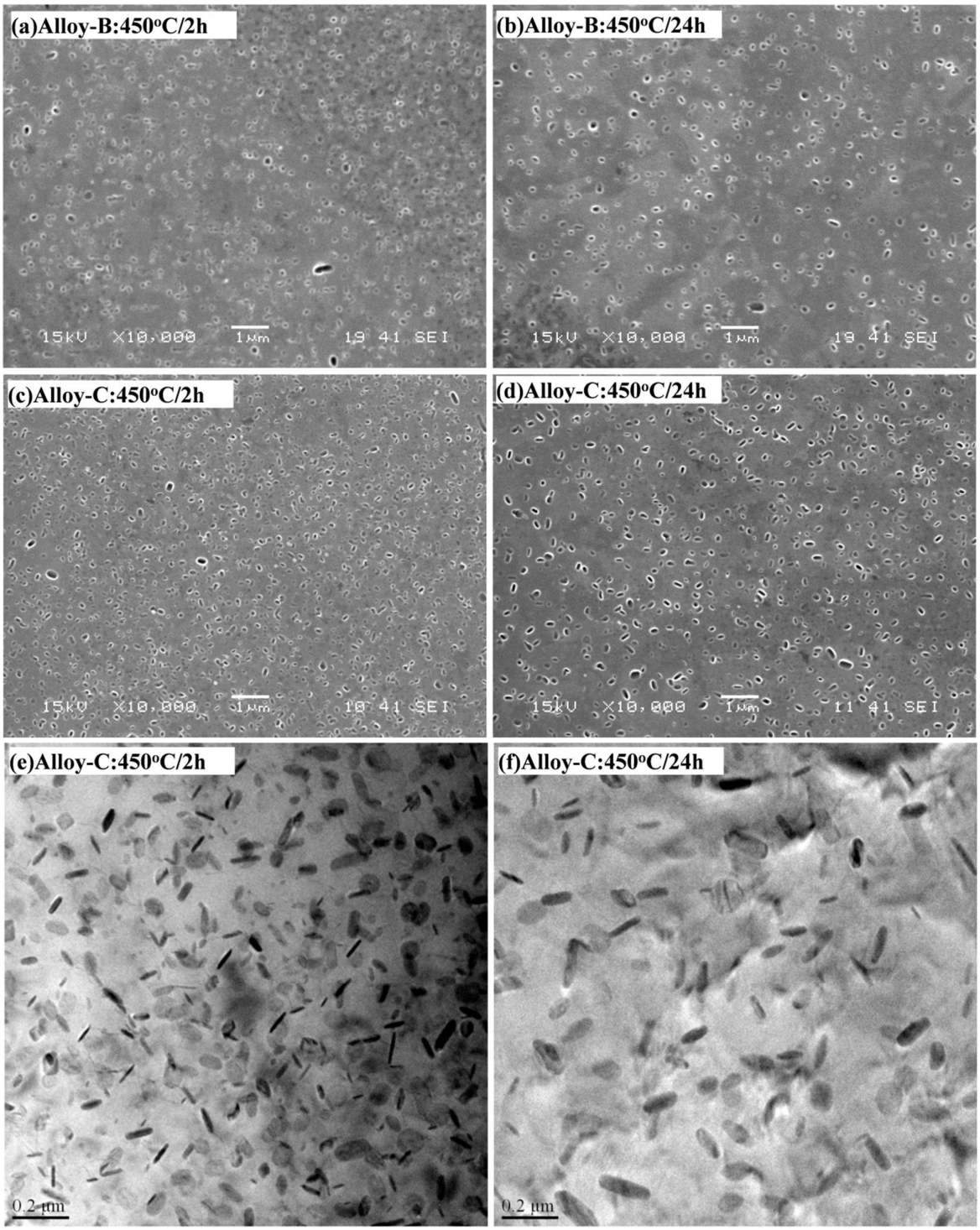

Fig. S2 Distribution of dispersoids at 450 ℃ in Alloys B and C